The conformation of acetylcholine at its target site in the membrane-embedded nicotinic acetylcholine receptor

P. T. F. Williamson*[†‡§], A. Verhoeven*, K. W. Miller[¶], B. H. Meier*, and A. Watts[‖]

*Physical Chemistry, ETH Zurich, Wolfgang-Pauli-Strasse 10, CH-8093 Zurich, Switzerland; [‖]Biomembrane Structure Unit, Biochemistry Department, University of Oxford, South Parks Road, Oxford 1 3QU, United Kingdom; [¶]Department of Biological Chemistry and Molecular Pharmacology, Harvard Medical School, and Department of Anesthesia and Critical Care, Massachusetts General Hospital, Blossom Street, Boston, MA 02114; [†]Centre National de la Recherche Scientifique; Strasbourg (LC3-UMR7177) and Montpellier (UMR-5048), France; and [‡]School of Biological Sciences, University of Southampton, Bassett Crescent East, Southampton SO16 7PX, United Kingdom

Edited by Ann E. McDermott, Columbia University, New York, NY, and approved September 25, 2007 (received for review May 22, 2007)

The conformation of the neurotransmitter acetylcholine bound to the fully functional nicotinic acetylcholine receptor embedded in its native membrane environment has been characterized by using frequency-selective recoupling solid-state NMR. Six dipolar couplings among five resolved ^{13}C-labeled atoms of acetylcholine were measured. Bound acetylcholine adopts a bent conformation characterized with a quaternary ammonium-to-carbonyl distance of 5.1 Å. In this conformation, and with its orientation constrained to that previously determined by us, the acetylcholine could be docked satisfactorily in the agonist pocket of the agonist-bound, but not the agonist-free, crystal structure of a soluble acetylcholine-binding protein from *Lymnaea stagnali*. The quaternary ammonium group of the acetylcholine was determined to be within 3.9 Å of five aromatic residues and its acetyl group close to residues C187/188 of the principle and residue L112 of the complementary subunit. The observed >C═O chemical shift is consistent with H bonding to the nicotinic acetylcholine receptor residues γY116 and δT119 that are homologous to L112 in the soluble acetylcholine-binding protein.

magic-angle spinning | membrane proteins | receptor pharmacology | solid-state NMR

It has been estimated that 45% of drugs in use today target membrane proteins (1, 2). In contrast to soluble proteins, the paucity and sometimes-low resolution of structural information for membrane proteins make rational drug design a distant dream. The Cys-loop pentameric ligand-gated ion channel (LGIC) family of proteins, which includes the $GABA_A$, glycine, nicotinic acetylcholine (ACh), and 5-HT_3 receptors, represents an important class of membrane receptors that are the targets of widely used and abused drugs. Typically these ≈250-kDa membrane receptors are gated by neurotransmitters of low molecular weight (≈100-Da). The archetypical and most intensively studied member of the LGIC superfamily is the muscle-type nicotinic ACh receptor (nAChR), which is composed of four homologous subunits arranged centrosymmetrically around a pore in the order α, δ, β, α, γ. The nAChR is found in the mammalian neuromuscular junction and in a highly enriched form in the electric organ of Torpedo, which provides a valuable source of receptor for biochemical and structural studies. Extensive studies have provided a wealth of information regarding the pharmacology of this family of receptors and identified putative residues which may be important in the binding of the agonist ACh (3, 4). Nonetheless, a precise structural understanding of how ACh binds to its binding site to gate the channel is still hindered by the quality of the structural data. To date, the best structural characterization of any intact LGIC is an electron microscopy structure of the Torpedo nAChR at 3.6 Å (5) in the resting, ligand-free state. Additionally, crystal structures at up to 2.0-Å resolution have been solved for soluble ACh-binding proteins (AChBPs) from *Lymnaea stagnalis* and *Aplysia californica* (6, 7). These proteins are frequently viewed as surrogates for the N-terminal agonist binding domain of the nAChR even though they exhibit only between 21% and 24% sequence identity with the α-subunit of the intact receptor and differ in their pharmacology (6, 7). Nevertheless, crystal structures of these AChBPs complexed with a range of agonists and antagonists (7, 8) have been refined to try and understand the pharmacology of the nAChR.

Both crystallography and solution-state NMR have been widely used in the characterization of ligand/receptor interactions, and although they represent the preferred route to the structural characterization of such systems (9, 10), their application to membrane proteins remains challenging. Although techniques for the analysis of low-affinity ligands binding to large membrane-receptor complexes have been developed (11), methods for the structural analysis of high-affinity ligands are still not widespread (12, 13). In contrast to solution-state NMR, which is limited by the overall size of the molecule, or crystallography, which requires the introduction of long range order in the sample, solid-state NMR, in principle, permits the measurement of structural constraints from the ligands bound to the receptor while resident within its native membrane (13). Here, we employ recently developed analysis techniques (14, 15) to determine multiple structural restraints for a uniformly labeled ligand by magic-angle spinning (MAS) rotational-resonance (RR) solid-state NMR. This approach allowed us to characterize the structure of the agonist ACh (Fig. 1*A*) while bound to the high-affinity desensitized state of the native nAChR from a single set of experiments, thus realizing a significant saving in the protein consumed over previous methods and removing the necessity to prepare multiple, site selectively labeled ligands. Combining these findings with the previously determined orientation of ACh (16), we have used a docking analysis to place ACh in the binding pocket of the high-resolution structure of the soluble AChBP, thus identifying ligand amino acid contacts necessary for binding. Such information is a prerequisite for the rational development of drugs against this class of membrane receptor.

Results

MAS NMR. To obtain well resolved spectra of ACh complexed with the nAChR, MAS NMR methods have been used to average the

Author contributions: P.T.F.W., K.W.M., B.H.M., and A.W. designed research; P.T.F.W. performed research; P.T.F.W. and A.V. contributed new reagents/analytic tools; P.T.F.W., A.V., K.W.M., B.H.M., and A.W. analyzed data; and P.T.F.W., A.V., K.W.M., B.H.M., and A.W. wrote the paper.

The authors declare no conflict of interest.

This article is a PNAS Direct Submission.

Abbreviations: ACh, acetylcholine; nAChR, nicotinic ACh receptor; MAS, magic-angle spinning; AChBP, ACh-binding protein; RR, rotational resonance; CP, cross-polarization; TPPM, two phase-pulse modulated.

[§]To whom correspondence should be addressed. E-mail: P.T.Williamson@soton.ac.uk.

This article contains supporting information online at www.pnas.org/cgi/content/full/0704785104/DC1.

© 2007 by The National Academy of Sciences of the USA

BIOPHYSICS

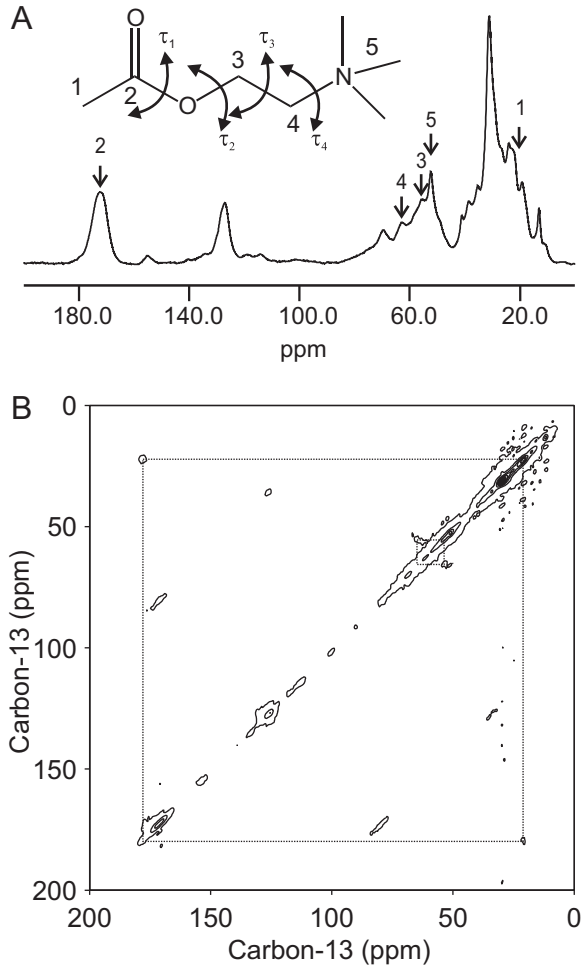

Fig. 1. CP-MAS spectrum of 20 nmoles of ^{13}C-labeled ACh bound to the nAChR recorded at 12.0 kHz with sites assigned to the five magnetically inequivalent ^{13}C-labeled carbons of bound ACh indicated by arrows. Spectrum averaged over 4,096 acquisitions and processed with 75 Hz line broadening. (*A*) (*Inset*) Structure of ACh and the numbering scheme of the carbons and torsion angles. Proton-driven spin-diffusion spectra (50 ms of mixing) of uniformly ^{13}C-labeled ACh bound to the nAChR. (*B*) Correlations between the adjacent carbon atoms are highlighted.

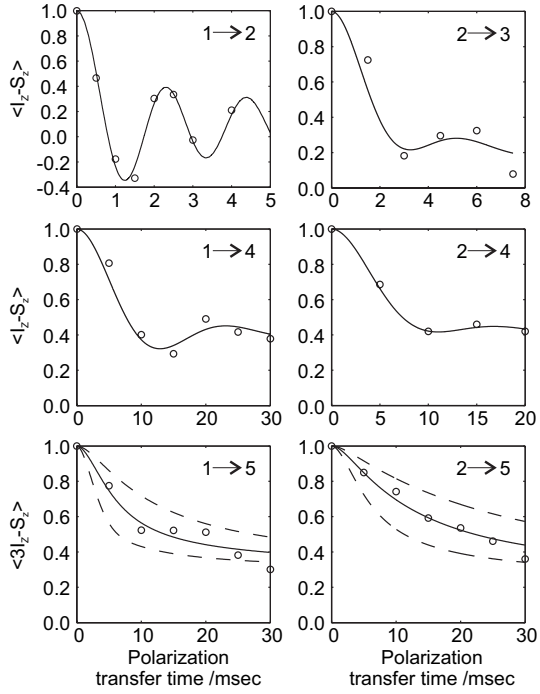

Fig. 2. Experimental RR polarization-transfer curves for 20 nmoles of uniformly ^{13}C-labeled ACh bound to the nAChR. Where a four-spin analysis has been used to determine the distances to site 5, exchange curves are plotted for the estimated distance (solid lines) together with those for ±0.5 Å of the estimated distance (dashed lines). All plots normalized to 1.0 at τ_m = 0 ms.

anisotropic interactions typically present in the spectra of biological membranes. A typical cross-polarization (CP) MAS spectrum of 20 nmoles of uniformly ^{13}C-labeled ACh bound to nAChR-rich membranes is shown in Fig. 1*A*. The spectrum of nAChR-enriched membranes is dominated by strong contributions from the natural abundance ^{13}C within the lipid and proteins present in the system, partially masking the resonances from the ^{13}C-labeled ACh bound to the nAChR. Four sites can, however, be resolved in a two-dimensional proton-driven spin diffusion experiment where off-diagonal correlations are observed between the adjacent ^{13}C atoms within the uniformly labeled ACh (Fig. 1*B*). Together with difference spectra obtained from samples with and without agonist, which permitted the assignment of the remaining resonance arising from the N-methyl group, the five chemically inequivalent sites of the bound agonist have been assigned (Fig. 1*A*). Their measured chemical shifts and the perturbation from those observed in crystalline ACh perchlorate are CO (178.0 ppm, +5.9 ppm); NCH_2 (66.5 ppm, +1.9 ppm); OCH2 (54.1 ppm, −3.6 ppm); $N(CH_3)_3$ (52.3 ppm, −1.6 ppm); and CH_3 (22.1 ppm, +2.6 ppm). These perturbations arise because of changes in the local electrostatic environment that are observed by the ligand upon binding and can reflect changes in both the ligand's local environment and its conformation (17). Although one should be cautious in the interpretation of the chemical shifts, we have previously been able to assign the upfield shift in the $N(CH_3)_3$ to the close proximity of aromatic groups within the receptor-binding site (17), while the strong downfield shift in the CO resonance is consistent with the formation of a strong H bond with groups within the ligand-binding site (18) [supporting information (SI) Fig. 5]. The specificity of this binding has been demonstrated by using the competitive irreversible inhibitor α-bungarotoxin, which confirmed earlier results obtained at 5°C demonstrating that the detected signals arise solely from ACh constrained within the agonist-binding site (17).

Structural Characterization by RR NMR. To determine the conformation of the uniformly ^{13}C-labeled ACh bound to the nAChR, multiple dipolar couplings between specific sites within the bound agonist have been determined to provide a direct measure of the distance between them. The dipolar couplings averaged under MAS can be selectively reintroduced by using RR NMR (19, 20). This technique relies on matching an integer multiple of the MAS frequency to the chemical-shift separation between the two sites that are being actively recoupled (19, 20). The dipolar coupling is obtained by monitoring the rate of polarization transfer between the two recoupled spins. The six polarization-transfer curves obtained for ACh while resident in its binding site on the nAChR are shown in Fig. 2. We were unable to determine all carbon–carbon distances for the bound ligand because of the unfavorable chemical shift separation between certain sites which would require unreasonably slow spinning (<1,000 Hz). Similarly, broadening of the methylene resonance and concomitant drop in signal to noise arising from the modest spinning speed required to fulfil the n = 1 RR condition prohibited the determination of the distance between sites 1 and 3.

Polarization-transfer curves have been used previously to determine internuclear distances for ligands in membrane targets (13, 21,

Table 1. Optimal parameters obtained from fits of the experimentally determined magnetization-exchange curves

Sites recoupled	Distance, Å	T_{2ZQ}, ms	Offset, Hz	Equilibrium population
2 to 3	2.55 ± 0.15	1.8	17.4	0.00
1 to 2	1.57 ± 0.04	5.0	0.0	0.01
2 to 4	3.69 ± 0.42	5.0	29.0	0.26
1 to 4	3.87 ± 0.26	7.2	0.0	0.34
1 to 5*	4.00 ± 0.50	1.6	10	0.0
2 to 5*	4.50 ± 0.50	1.6	30	−0.1

T_{2ZQ} is the phenomenological constant describing the decay of the zero-quantum coherence. Offset and equilibrium population describe the offset from the RR condition and final equilibrium polarization required to compensate for the presence of passively coupled spins, as described in refs. 14 and 15. Errors reported are those given by MINUIT and represent one standard deviation.

*Distance and relaxation rates obtained from an analysis of a four-spin system. Errors determined from the analysis of the χ^2 surface.

22), however, these studies have relied on the incorporation of an isolated spin pair to facilitate the analysis, and thus the characterization of the global conformation required the preparation of multiple double-labeled ligands. We have recently described how to extract the dipolar couplings between the actively recoupled spins in a uniformly labeled sample, allowing perturbations arising from passive spins that may influence the polarization transfer to be accommodated (15, 23). We have used this analysis to extract the internuclear distance between pairs of ^{13}C nuclei in uniformly labeled ACh while accommodating the effects of additional close-by ^{13}C. The free parameters of the data analysis are the dipolar coupling between the actively recoupled spins, the zero-quantum relaxation rate (T_{2ZQ}), and an effective offset for the RR condition arising from the passively coupled spins. Fitting this model to the experimental data (Fig. 2 and Table 1) shows that under the experimental conditions used here, the distances between the spin pairs can be determined with a statistical error of less than ±0.5 Å. It is noted that with such analyses, systematic errors may occur, however, analysis of the crystalline ACh perchlorate (15) (see *SI Text* and SI Figs. 6–8) indicate that, in unfavorable circumstances, these are of the order of ±0.2 Å.

To analyze polarization transfer among the three methyls at site 5 giving rise to a single resonance line and the methyl at site 1 or the carbonyl at site 2 (see Fig. 1*A*), we have used a numerical analysis scheme (described below). This analysis gives the distance between the spins at sites 1 or 2 and the three spins of site 5 at a "pseudoatom" located at the geometric center between the three methyl groups attached to the quaternary ammonium. At the temperatures at which these experiments were performed earlier, ^2H NMR studies (16) indicate the quaternary ammonium group is free to rotate in the binding site, suggesting that on the time scale of the experiments, an averaged dipolar coupling would be observed. We assume that the distances from sites 1 or 2 to this pseudoatom are related by the normal dipolar coupling constant with an r^{-3} dependence. This assumption may systematically under- or overestimate the distance obtained from the measurements because the dipolar nature of the interaction requires averaging over r^{-3} and the angular dependence according to $3\cos^2\theta - 1$ depending on the actual conformation of the molecule. This error, however, stays well within the limits applied in our data analysis. The χ^2 deviation between the measured exchange and a grid of simulated exchange curves in a parameter space spanning the dipolar coupling frequency, T_{2ZQ}, the effective offset from RR condition, and the offset in equilibrium polarization was calculated (see SI Fig. 9). Analysis of this χ^2 surface revealed that deviations larger than ±0.5 Å in the distance (from sites 1 or 2 to site 5) would be inconsistent with the observed polarization-transfer curves (see dashed lines in Fig. 2). Similar analysis of the crystalline ACh perchlorate revealed discrepancies between the NMR and x-ray-derived distances of up to 0.32 Å (see *SI Text*).

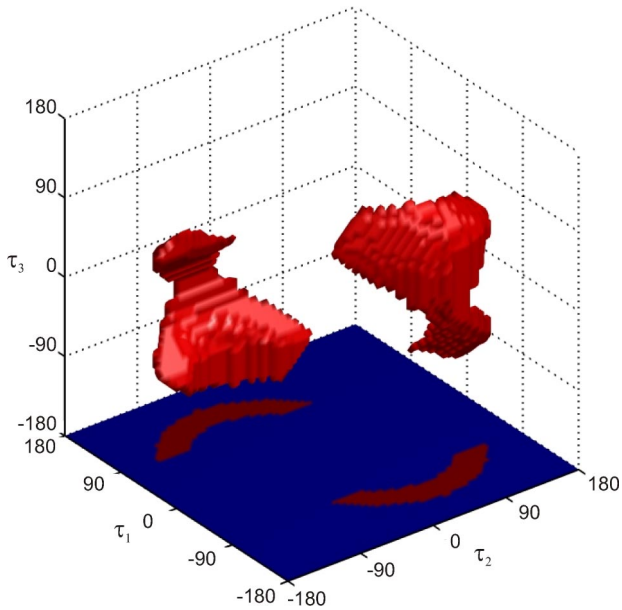

Fig. 3. Plot of the torsion angle space τ_1, τ_2, τ_3 with the volumes containing structures consistent with all six NMR-derived constraints (within ±1 standard deviation) highlighted in red.

Structural Refinement of Bound ACh. The conformation of ACh can be defined in terms of four torsion angles (see Fig. 1*A*); although τ_4 remains undefined because of the rotation of the quaternary ammonium group. To obtain a family of structures consistent with the measured NMR constraints, a systematic search of the torsion-angle space (τ_1, τ_2, τ_3) was performed, of which 1.5% of the structures that were generated were consistent with the observed NMR constraints within ±1 standard deviation of the measured distances given in Table 1. The structures that fulfill all six NMR constraints are enclosed within the volumes highlighted in red in Fig. 3. This analysis reveals two families of structures related by symmetry; the first is characterized by the average torsion angles of 52°, −128°, and 62° and the second by average torsion angles of −52°, 128°, and −62° (Fig. 4*A*). In torsion-angle space, these values are not all well defined, because rather small errors in the distance measurements can, for some angles, propagate into a rather large spread in consistent torsion angles (Fig. 3). In contrast, a root mean squared deviation (rmsd) analysis of the superimposed structures (Fig. 4*A*), which enables the consideration of the errors in all of the distance measurements on the entire ensemble, reveals an rmsd of 0.40 Å for the heavy atoms (C, N, O). If the quaternary ammonium group is excluded from the rmsd analysis, this figure falls to 0.28 Å and represents the figure one would expect if this analysis was applied to ligands that do not contain sites of magnetic equivalence. The higher rmsd when the quaternary ammonium group is included is a consequence of the higher uncertainty associated with the numerical treatment of the spin dynamics (see *Methods* and *SI Text*).

From the distance data collected, we were unable to distinguish between the two mirror-symmetric conformations. However, in both cases, the methyl group (site 1) is folded back toward the quaternary ammonium group (site 5), resulting in a condensed structure where some τ_4 values result in unfavorable Van der Waals contacts between the two sites and an energy barrier of 66 kJ mol^{-1} for the free rotation of the quaternary ammonium group. These observations agree with previous deuterium NMR studies of bro-

BIOPHYSICS

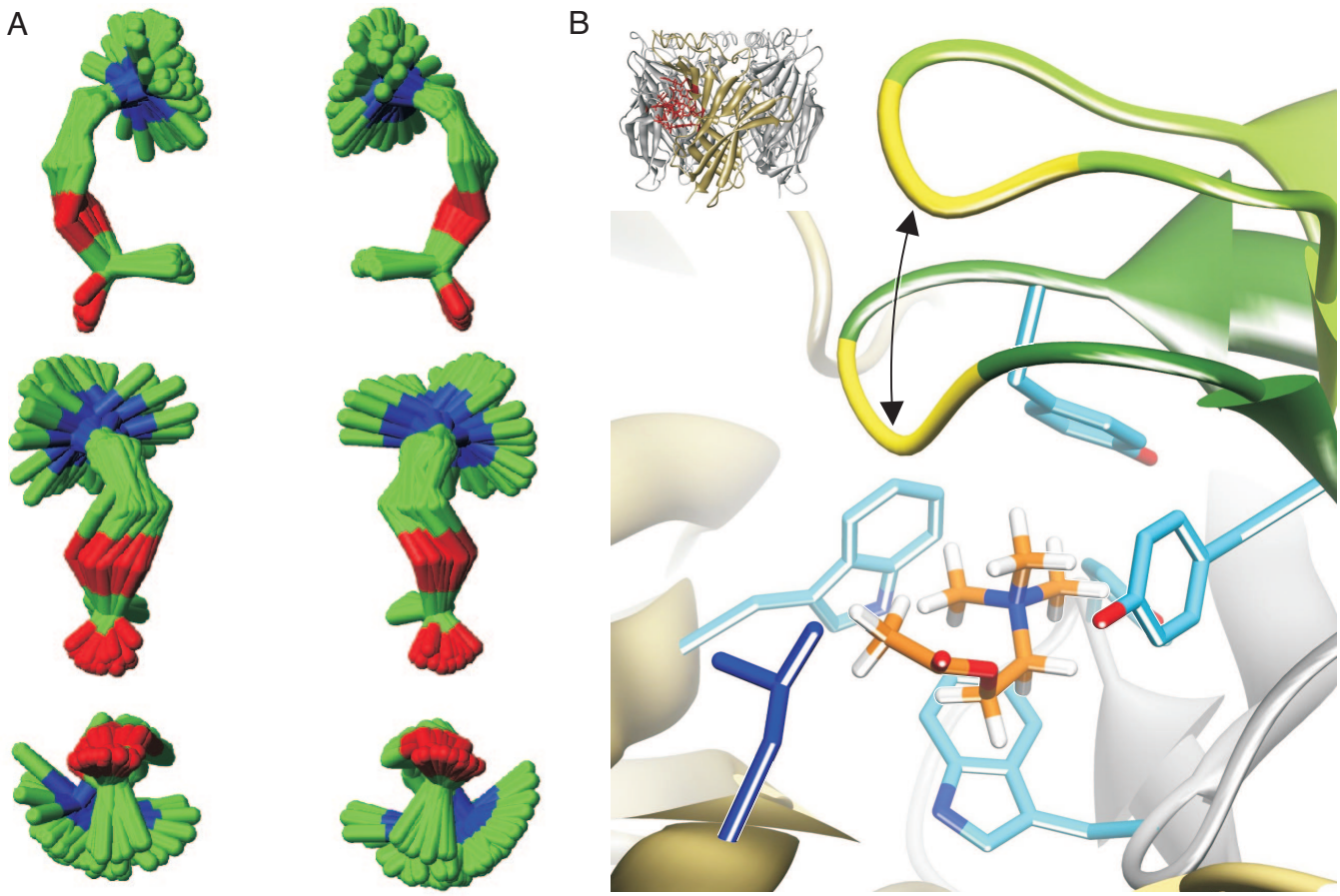

Fig. 4. The two symmetry-related families, shown in three orthogonal projections, identified from the analysis of all possible structures consistent with all NMR constraints for ACh bound to the agonist-binding site on the desensitized nAChR. (*A*) Each family shown is the minimum rmsd superimposition of the heavy atoms (excluding the methyl carbons attached to the quaternary ammonium group) of 20 randomly chosen samples from the consistent structures. (*B*) Lowest energy model of the ACh ($\tau_1 = -53°$; $\tau_2 = 128°$; $\tau_3 = -62°$) docked to the homologous AChBP (1UV6). (*Inset*) The position of the detailed view on the AChBP is shown in red. Aromatic side chains within 3.9 Å of the bound ACh are shown in medium blue to highlight the aromatic pocket involved in the binding of the quaternary ammonium group. The leucine (dark blue, left foreground) on the complementary subunit (sandy colored) is γY116 or δT119 in the ACh receptor. These residues are well located to H-bond to ACh's carbonyl group. The C-loop (green), which contains the vicinal disulphide bond (yellow), folds around the ACh completing the aromatic pocket and bringing the cysteines into close proximity to the methyl group of the ligand. The C-loop of the unliganded AChBP from *A. californica* (shown in light green) is superimposed on our model of the ACh docked to the AChBP, demonstrating how the C-loop folds around the ACh upon binding.

moacetylcholine within the binding site (16) and suggest that ACh binding results in conformational changes that hinder the free rotation of the quaternary ammonium group as observed in earlier ^{2}H spectra (16), with little hindrance from interactions with the binding site.

Docking Analysis of ACh with the AChBP. To determine how the ACh interacts with the nAChR, we performed a series of docking analyses. In contrast to earlier docking studies in which the ligand conformation is unknown, in this work we fixed the torsion angles to those determined from the NMR distance constraints and the orientation to that observed in earlier deuterium NMR studies (17). This approach enabled us to see how the residues within the ligand-binding site mold themselves around the ligand. Crystal structures are available for the native-, nicotine-, and carbamylcholine-bound forms of the AChBP at 2.5 Å together with a 3.6-Å cryoelectron microscopy structure of the intact nAChR (6–8). Analysis of 100 docked structures of ACh bound to either the AChBP or the nAChR, both in their low-affinity native conformations, showed that the position of the ligand was poorly defined within the binding site with relatively low binding energies. In contrast, our NMR-derived structure docked to the carbamylcholine-bound form of the AChBP with the carbamylcholine removed is in a relatively well defined position with a 6-fold higher affinity than when bound to the native AChBP or nAChR. Of the 100 complexes derived for each of the two ACh conformations, the lowest energy structures placed the quaternary ammonium group within 3.9 Å of five aromatic residues, four of them from the principle subunit of the binding site in the AChBP, namely Y89(Y93), W143(W149), Y185(Y190), and Y192(Y198) (homologous residues' numbers from the α-subunit of the nAChR from *Torpedo californica* are given in brackets), and the fifth, W53(W55), contributed from the "complementary" subunit (Fig. 4*B*). In contrast to the relatively well defined nature of the quaternary ammonium group, the acetyl group showed more variation in its positioning within the binding site, in agreement with recent molecular dynamics calculations (24). However, for the lowest energy complexes, the acetyl group was found in close proximity to C187/188(C192/193) of the principle subunit and L112 and M114 of the complementary subunit. In this position, the docked ACh has a similar orientation to that observed in the crystal structure of carbamylcholine in the binding site on the AChBP (8); however, because of the differing torsion angles, the C-methyl group is positioned closer to C187/188(192/193) than the corresponding amine in the carbamylcholine.

Discussion

Pharmacological studies of ACh and its analogues have identified at least two key pharmacophores involved in the binding of ACh to the nAChR, the positively charged quaternary ammonium group and a center of electronegativity to act as an H-bond acceptor. Early studies indicated that the distance between the positively charged nitrogen and the Van der Waals surface of the carbonyl oxygen should be ≈5.9 Å for optimal binding to the nAChR (25). The distance between the positively charged nitrogen and the carbonyl measured from our NMR derived structure is 5.1 Å. This measurement corresponds to a distance of 6.1 Å when measured to the Van der Waals surface of the carbonyl oxygen, in good agreement within the expected errors. Docking studies performed on homology models of the α_7 and the $\alpha_2\beta\gamma\delta$ nAChRs (26) also reveal a similar spatial positioning with the two pharmacophores separated by 5.33 Å, which is in agreement with that observed in our NMR-derived structures.

Studies of rigid analogues, including lophotoxin (27), have characterized the torsion angles required for optimal binding to the nAChR with molecular dynamics studies of the structurally constrained lophotoxin indicating the torsion angles τ_1, τ_2, and τ_3 of $-9°$, 138°, and $-61°$ with other analogues giving values within $\pm 10°$ of these. This confirmation results in a similar spatial positioning of the pharmacophores to that found in our structure of the bound ACh and results in similar torsion angles with the exception of τ_1, where a discrepancy of 40° is observed (27).

The docking studies of ACh bound to the native AChBP and to the resting-state nAChR performed here revealed relatively low binding affinities in comparison to those observed for similar studies of the carbamylcholine-bound conformation of the AChBP. This result is in agreement with the known affinities of these conformations. Analysis of the positioning of the two pharmacophores identified as necessary for high-affinity ACh binding indicates that the quaternary group is in close proximity to the aromatic residues Y89(Y93), W143(W149), Y185(Y190), and Y192(Y198). This is consistent with earlier chemical-labeling studies using ACh mustard (28), a close analogue of ACh that reacts with Y89(Y93), and other photoreactive analogues of competitive antagonists which have been shown to react with W143(W149), Y185(Y190), and Y192(Y198) (29–32). It also highlights the importance of these residues for the formation of cation–π interactions that stabilize the positively charged quaternary ammonium group within the binding site (33) and are vital for binding ACh to the nAChR. In contrast, the variability in the positioning of the acetyl group of the ACh precludes the identification of a suitable H-bonding partner for the carbonyl group of the ACh, even though the acetyl group is in close proximity to C187/188(C192/193), which has been identified in chemical-labeling experiments. This observation is inconsistent with the large perturbations observed in the carbonyl chemical shift that we observed upon ligand binding (+5.9 ppm), which supports earlier pharmacological studies suggesting the importance of an H-bond in high-affinity ACh binding and a more restrained position for the acetyl group. The absence of such an H-bond partner in the homomeric AChBP, which has been used in our docking studies, is consistent with its relatively low affinity for ACh, just as it is in homomeric α_7 receptors (34). However, the docking places the carbonyl group in close proximity to L112 of the complementary subunit (blue in Fig. 3*B*) corresponding to Y116 and T119 of the γ- and δ-subunits of the heteromeric ($\alpha_2\beta\gamma\delta$) nAChRs studied here (35). Both of these groups have previously been identified by photoaffinity labeling with (+)-Tubocurarine (35, 36) and could provide the H-bond donors necessary for the high-affinity binding of ACh to these heteromeric receptors, accounting for the perturbations in chemical shift that we observe for the bound ligand. To maximize the interaction between the ligand and binding site, the C-loop has folded around the ACh within the binding site, bringing the vicinal disulphide bond (yellow residues in Fig. 4*B*) in close proximity to the methyl group of the ligand, which is in agreement with chemical-labeling studies (37, 38). This change is shown in Fig. 4*B*, where the C-loop (shown in green/yellow) of the native AChBP from *A. californica* is superimposed on top of our model of the AChBP with ACh bound. The observed changes in structure are similar to the differences found between the native and Epibatidine forms of the AChBP from *A. californica*, where a similar folding of the C-loop around the small agonist is observed (7). These changes have been proposed to be an essential part of the conformational changes resulting in the formation of both the active and desensitized states.

In this study, frequency-selective recoupling techniques have been used to obtain multiple distance restraints from a uniformly labeled ligand while bound to a membrane receptor complex. This method has two practical advantages over methods using ligands that are selectively labeled. First, only a single isotopically substituted ligand need be synthesized. Second, and most importantly, the ability to extract the results from a single experiment requires much less protein to achieve the goal. Given the difficulty of overexpressing membrane proteins, this method effectively extends the range of proteins to be studied (13).

The structural characterization of the bound ACh combined with docking analysis of the ligand to the homologous AChBP is sufficient to characterize many of the interactions necessary for ligand binding and their relative spatial arrangement. In combination with other MAS-NMR techniques that identify residues in close proximity to the ligand (39), such studies have the potential to characterize the pharmacophores involved in the binding of small molecules to membrane receptors as a prerequisite to the rational development of new pharmaceuticals (13).

Methods

Sample Preparation. nAChR-enriched membranes from *Torpedo nobiliana* were prepared for NMR as described in ref. 17 and typically contained 0.8 nmoles of binding site per milligram of protein. Samples corresponding to 25 mg of protein were loaded into a 4-mm MAS rotor and sealed. Uniformly labeled ACh was prepared as described in ref. 17, 20 nmoles were added to the membrane pellet as a small aliquot before the experiments and allowed to equilibrate (4°C, 30 min).

NMR Spectroscopy. All ^{13}C MAS spectra were recorded on a Varian Infinity + 500 MHz spectrometer (Varian, Palo Alto, CA) equipped with a 4-mm double resonance MAS probe. Carbon magnetization was generated by using an adiabatic CP scheme with a ^{13}C spin-lock field of 70 kHz. Protons were decoupled during polarization exchange and acquisition by using 120 kHz two phase-pulse modulated (TPPM) decoupling (40). Polarization transfer between the actively recoupled spins was measured by using a one-dimensional polarization-exchange experiment as described in refs. 15 and 23. Briefly, after CP, one of the actively recoupled sites was selectively inverted by using a delay alternating with nutation for tailored excitation (DANTE) scheme and subsequently allowed to exchange for a given time before being monitored by a $\pi/2$ readout pulse. To enhance the fidelity with which the transferred polarization was measured, after the acquisition of polarization transfer, an acquisition without transfer was acquired and subtracted. The spinning frequency was set to be equal to the chemical-shift difference between the two sites to be recoupled (half of this value for the $n = 2$ experiment between sites 1 and 2). The sample was kept at a constant temperature of -50°C (value estimated from calibration data with an uncertainty of ± 5°C), enhancing sensitivity and preventing possible sample degradation. Each point in the polarization-transfer curves represents the sum of 32,768 difference experiments. Proton-driven spin diffusion spectra were acquired with an exchange experiment by using CP to generate ^{13}C polarization and TPPM decoupling during both acquisition periods. Phase-sensitive data were acquired by using time-proportional

phase incrementation (TPPI) with 256 slices in the indirect dimension; each slice is the result of 256 acquisitions. Line broadening (100 Hz) was applied in both dimensions.

Data Analysis. Polarization-transfer curves were analyzed by using the model described in refs. 14 and 15. Spin simulations were performed with the GAMMA spin-simulation environment (41) and fitted by using the analysis package MINUIT (42). Fitted parameters include the distance between the actively recoupled spins, the zero-quantum relaxation rate, the effective offset from the RR condition, and the offset in final equilibrium polarizations (14, 15). Polarization transfer under RR has been shown to depend on the chemical-shielding anisotropy and the relative orientation of the anisotropic interactions. These effects are known to be small at the $n = 1$ recoupling condition chosen here and within the time frame under which the polarization transfer has been observed (20). This simplified analysis avoids the necessity for exhaustive numerical simulations that are both computationally demanding and reliant on a detailed knowledge of both the isotropic and anisotropic interactions and their relative orientations that describe the spin system, information which presumes a detailed knowledge of the structure. With reference to our earlier studies using this method, the analysis presented here uses both an offset from the RR condition and an equilibrium polarization difference to account for any discrepancies in equilibrium difference polarization that may arise during the normalization of the data. Direct comparisons with previous published models (14, 15) indicate that any discrepancies are within the statistical errors reported here.

Analysis of the polarization transfer between the three methyls at the quaternary ammonium group (site 5) and the single carbons at sites 1 and 2 was performed by comparing the experimental results to numerical Liouville-space simulations of a four-spin system by using the GAMMA spin-simulation environment (41). The system was modeled as three magnetically equivalent nuclei spaced equidistantly to a fourth spin. Contributions from chemical-shielding anisotropies were ignored, as were couplings between the N-methyl carbons which were shown to have no effect on the RR polarization transfer between sites 1 and 2 and site 5. Relaxation was implemented as an uncorrelated random field fluctuation along the z-direction, with an identical rate constant for each spin. Because of the computational demands of these simulations, the data were analyzed by using a systematic search of a parameter space spanning the dipolar coupling, T_{2ZQ}, offset from RR condition and offset in equilibrium polarization. Variation of the offset from RR condition and offset in equilibrium polarization allowed contributions from the coupling to passive spins to be included in a manner analogous to the two-spin simulations. Errors were estimated from an analysis of the χ^2 surface.

Structure Determination and Ligand Docking. Structures consistent with the determined distance constraints were identified by a systematic search of a basis set of conformers generated by systematically varying the torsion angles τ_1, τ_2, and τ_3 in 5° steps by using Discover 95.0 (Accelrys, San Diego, CA). Structures consistent with all of the experimentally determined constraints within one standard deviation were included in the subsequent rmsd analysis.

The two average structures that were determined were docked to the crystal structure of the AChBP complexed with carbamylcholine (1UV6). Before docking, the carbamylcholine was removed from the binding site. The two ACh conformers were docked to the AChBP 100 times by using the cvff force field in Discover 95.0 (Accelrys). Initially, the ligand was placed with a random position and orientation and was subject to 100 rounds of conjugate-gradient minimization by using a nonbond potential containing only scaled (10%) Van der Waals interactions (quartic without coulomb). The structures were then subject to another 200 rounds of conjugate-gradient minimization by using the cell-multipole method to characterize the nonbond interactions. Torsion angles and relative orientation of the C–N bond were restrained by using a cosine penalty function and the ligand was tethered to within 10 Å of the binding site by using a flat-bottomed penalty function. With the exception of residues within 10 Å of carbamylcholine in the original crystal structure, all residues were fixed.

We thank Dr. M. Ernst and Dr. G. Gröbner for the many useful discussions. This work was supported in part by the Medical Research Council (U.K.) Engineering and Physics Research Council (A.W.), the Swiss National Science Foundation (B.H.M. and P.T.F.W.), the Biotechnology and Biological Sciences Research Council Cooperative Awards in Science and Engineering (GlaxoWellcome), Centre National de la Recherche Scientifique/Action Jeunes Cherchers Grant UMR7177/UMR5048, a Research Career Development Fellowship from the Wellcome Trust (P.T.F.W.), and the National Institutes of Health Grant GM 58448 (to K.W.M.).

1. Terstappen GC, Reggiani A (2001) *Trends Pharmacol Sci* 22:23–26.
2. Drews J (2000) *Science* 287:1960–1964.
3. Karlin A (1993) *Curr Opin Neurobiol* 3:299–309.
4. Arias HR (1997) *Brain Res Rev* 25:133–191.
5. Miyazawa A, Fujiyoshi Y, Unwin N (2003) *Nature* 423:949–955.
6. Brejc K, van Dijk WJ, Klaassen RV, Schuurmans M, van der Oost J, Smit AB, Sixma TK (2001) *Nature* 411:269–276.
7. Hansen SB, Sulzenbacher G, Huxford T, Marchot P, Taylor P, Bourne Y (2005) *EMBO J* 24:3635–3646.
8. Celie PHN, van Rossum-Fikkert SE, van Dijk WJ, Brejc K, Smit AB, Sixma TK (2004) *Neuron* 41:907–914.
9. Blundell TL, Jhoti H, Abell C (2002) *Nat Rev Drug Discovery* 1:45–53.
10. Pellecchia M, Sem DS, Wurthrich K (2002) *Nat Rev Drug Discovery* 1:211–219.
11. Roberts GCK (2000) *Drug Discovery Today* 5:230–240.
12. Watts A, Burnett IJ, Glaubitz C, Gröbner G, Middleton DA, Spooner PJR, Williamson PTF (1998) *Eur Biophys J Biophys Lett* 28:84–90.
13. Watts A (2005) *Nat Rev Drug Discovery* 4:555–568.
14. Williamson PTF, Verhoeven A, Ernst M, Meier BH (2003) *J Am Chem Soc* 125:2718–2722.
15. Verhoeven A, Williamson PTF, Zimmermann H, Ernst M, Meier BH (2004) *J Magn Reson* 168:314–326.
16. Williamson PTF, Watts JA, Addona GH, Miller KW, Watts A (2001) *Proc Natl Acad Sci USA* 98:2346–2351.
17. Williamson PTF, Gröbner G, Spooner PJR, Miller KW, Watts A (1998) *Biochemistry* 37:10854–10859.
18. Ando I, Kameda T, Asakawa N, Kuroki S, Kurosu H (1998) *J Mol Struct* 441:213–230.
19. Levitt MH, Raleigh DP, Creuzet F, Griffin RG (1990) *J Chem Phys* 92:6347–6364.
20. Raleigh DP, Levitt MH, Griffin RG (1988) *Chem Phys Lett* 146:71–76.
21. Middleton DA, Robins R, Feng XL, Levitt MH, Spiers ID, Schwalbe CH, Reid DG, Watts A (1997) *FEBS Lett* 410:269–274.
22. Verdegem PJE, Bovee-Geurts PHM, de Grip WJ, Lugtenburg J, de Groot HJM (1999) *Biochemistry* 38:11316–11324.
23. Williamson PTF, Ernst M, Meier BH (2003) in *BioNMR in Drug Research*, ed Zerbe O (Wiley-VCH, Weinheim, Germany) pp 243–282.
24. Henchman RH, Wang HL, Sine SM, Taylor P, McCammon JA (2005) *Biophys J* 88:2564–2576.
25. Beers WH, Reich E (1970) *Nature* 228:917–922.
26. Le Novere N, Grutter T, Changeux JP (2002) *Proc Natl Acad Sci USA* 99:3210–3215.
27. Taylor P, Abramson SN, Johnson DA, Fernando Valenzuela C, Herz J (1991) *Ann NY Acad Sci* 625:568–587.
28. Cohen JB, Sharpe SD, Liu WS (1991) *J Biol Chem* 266:23354–23364.
29. Chiara DC, Cohen JB (1997) *J Biol Chem* 272:32940–32950.
30. Dennis M, Giraudat J, Kotzbya-Hibert F, Goeldner M, Hirth C, Chang JY, Lazure C, Chretien M, Changeux JP (1988) *Biochemistry* 27:2346–2357.
31. Galzi JL, Revah F, Black D, Goeldner M, Hirth C, Changeux JP (1990) *J Biol Chem* 265:10430–10437.
32. Langenbuch J, Bon C, Mulle C, Goeldner M, Hirth C, Changeux JP (1988) *Biochemistry* 27:2337–2345.
33. Ma JC, Dougherty DA (1997) *Chem Rev (Washington, DC)* 97:1303–1324.
34. Costa V, Nistri A, Cavalli A, Carloni P (2003) *Br J Pharmacol* 140:921–931.
35. Karlin A (2002) *Nat Rev Neurosci* 3:102–114.
36. Chiara DC, Xie Y, Cohen JB (1999) *Biochemistry* 38:6689–6698.
37. Silman I, Karlin A (1969) *Science* 164:1420–1421.
38. Kao P, Dwork A, Kaldany R, Silver M, Wideman J, Stein S, Karlin A (1984) *J Biol Chem* 259:11662–11665.
39. Kiihne S, Creemers AFL, de Grip WJ, Bovee-Geurts PHM, Lugtenburg J, de Groot HJM (2005) *J Am Chem Soc* 127:5734–5735.
40. Bennett AE, Rienstra CM, Auger M, Lakshmi KV, Griffin RG (1995) *J Chem Phys* 103:6951–6958.
41. Smith SA, Levante TO, Meier BH, Ernst RR (1994) *J Magn Reson A* 106:75–105.
42. James F (1994) in *European Center for Nuclear Research (CERN)* Program Library Entry D506 (European Center for Nuclear Research, Geneva).